Proceedings of the 2009 IEEE International Conference on Systems, Man, and Cybernetics
San Antonio, TX, USA - October 2009

Underwater Target Detection from Multi-Platform Sonar Imagery Using Multi-Channel Coherence Analysis

Nick Klausner, Mahmood R. Azimi-Sadjadi, and J. Derek Tucker
Department of Electrical and Computer Engineering
Colorado State University
Fort Collins, Colorado, 80523, USA
nklausne@engr.colostate.edu

***Abstract*—This paper introduces a new target detection method for multiple disparate sonar platforms. The detection method is based upon multi-channel coherence analysis (MCA) framework which allows one to optimally decompose the multi-channel data to analyze their linear dependence or coherence. This decomposition then allows one to extract MCA features which can be used to discriminate between two hypotheses, one corresponding to the presence of a target and one without, through the use of the log-likelihood ratio. Test results of the proposed detection system were applied to a data set of underwater side-scan sonar imagery provided by the Naval Surface Warfare Center (NSWC), Panama City. This database contains data from 4 disparate sonar systems, namely one high frequency (HF) sonar and three broadband (BB) sonars coregistered over the same area on the sea floor. Test results illustrate the effectiveness of the proposed multi-platform detection system in terms of probability of detection, false alarm rate, and receiver operating characteristic (ROC) curves.**

***Index Terms*—binary hypothesis testing, disparate sonar platforms, multi-channel coherence analysis, underwater target detection**

I. Introduction

Underwater Target Detection from Multi-Platform Sonar Imagery Using Multi-Channel Coherence Analysis The development of a robust underwater target detection and classification system that can operate with multiple disparate sensor systems and in different operating conditions poses many technical challenges. In the traditional centralized processing, preliminary detection, feature extraction and object classification are performed based upon the data collected using every sensor platform. A final decision-making usually takes place at the central station, either in the post-mission analysis (PMA) or real-time network-centric sensor analysis (NSA) modes, using some type of a decision, feature or combined fusion mechanism. However, decision-making based upon individual sensory data typically leads to incomplete, degraded or biased local (sensor-level) decisions hence resulting in an unacceptable final detection and classification performance at the fusion center.

In the collaborative decision-making using several sensor platforms, it is essential to detect and further scrutinize the information-bearing parts of the data collected by various platforms. This involves detecting, isolating and representing, in terms of some pertinent attributes, the *coherent* or common information among the multiple data sets. This is an extremely challenging problem due to the disparate nature of the problem and variations in the operating conditions. Thus, to develop a system-level solution, new methodologies are needed to: (a) collaboratively detect and agree on threats occurring within the field of view of the sensors, (b) perform collaborative feature extraction to capture common target attributes from multiple sensor platforms, (c) perform object classification and identification, (d) and finally develop a single integrated target assessment picture based upon the detected, localized and classified targets from multiple disparate sensors.

The existing work [1] - [2] in the area of target detection from sonar imagery has primarily been focused on one sonar platform, with fusion across multiple algorithms. In [3], the adaptive clutter filter detector in [2] is individually applied to three different sonar images varying in frequency and bandwidth. Final classification is done using an optimal set of features using a nonlinear log-likelihood ratio test where the decisions of the individual detector and classifier are fused. The optimal set of features is determined based upon cascading another classifier on the previous classifier during the training stage. This is done as a repeated application during the training stage where at each iteration the threshold and optimal feature set is chosen and updated. In our previous work [4], we developed a new framework for dual-sensor coherence analysis using Canonical Coordinate Analysis (CCA) [5], [6] that can be applied to the data collected using two disparate sonar systems. Using this method allows for the simultaneous detection and feature extraction of coherent target information among two sonar images. The CCA data channels consist of ROI's from the two co-registered sonar images. The *detection hypothesis* in this framework is that the presence of objects in the two-platform sonar data leads to a high level of coherence measure compared to that of background clutter.

This paper extends the work in [4] to an N-channel coherence-based detector using the Multi-Channel Coherence Analysis (MCA) framework. As with [4], the N-channel Gauss-Gauss detector is formulated in the MCA framework,

978-1-4244-2794-9/09/$25.00 ©2009 IEEE

exploiting the coherence of objects present in N disparate channels or sonar data sets. This is due to the fact that the presence of objects in the co-registered multi-platform sonar data leads to a higher level of coherence compared to that of background clutter alone. New expressions for the log-likelihood ratio and J-divergence [6] in the MCA framework are provided that can be used for the simultaneous detection of targets using N disparate sonar platforms. The proposed detection framework is then implemented using a data set provided by the NSWC - Panama City that consists of a HF and three BB side-looking sonar imagery coregistered over the same region on the sea floor.

This paper is organized as follows: Section II will review the MCA framework. Section III develops the MCA-based Gauss-Gauss detection method. Section IV provides the results of implementing the proposed detector on the NSWC data set and finally concluding remarks will be made in Section V.

II. A Review of Multi-Channel Coherence Analysis [7]

Consider N zero mean random vectors, $\mathbf{x}_1$, $\mathbf{x}_2$,..., and $\mathbf{x}_N$, representing multiple data channels comprising the composite data channel $\mathbf{z} = [\mathbf{x}_1^H \mathbf{x}_2^H ... \mathbf{x}_N^H]^H \in \mathbb{C}^{d\times 1}$. Without loss of generality, we will assume all random vectors to be zero mean throughout this analysis. Let each channel $\mathbf{x}_j \in \mathbb{C}^{d_j \times 1}$ be of dimension d_j, where it is assumed that $\mathbf{x}_1$ is of the smallest dimension and we denote $d = \sum_{j=1}^{N} d_j$. The $d \times d$ dimensional covariance matrix of the composite data channel $\mathbf{z}$ is given by

$$R_{\mathbf{zz}} = E\left[\mathbf{z}\mathbf{z}^H\right] = \begin{bmatrix} R_{11} & R_{12} & \cdots & R_{1N} \\ R_{21} & R_{22} & \cdots & R_{2N} \\ \vdots & \vdots & \ddots & \vdots \\ R_{N1} & R_{N2} & \cdots & R_{NN} \end{bmatrix}, \quad (1)$$

where $R_{jk} = E[\mathbf{x}_j \mathbf{x}_k^H]$ is the auto-covariance ($j = k$) or cross-covariance ($j \neq k$) matrices of data channels $\mathbf{x}_j$ and $\mathbf{x}_k$ and clearly we have $R_{jk} = R_{kj}^H$.

Similar to CCA [8], [9] the ith multi-channel coordinate of the jth channel is found by searching for the ith coordinate mapping vector, $\boldsymbol{\alpha}_{i,j}$, of data channel $\mathbf{x}_j$. This linear transformation produces the ith multi-channel coordinate for the jth channel,

$$v_{ij} = \boldsymbol{\alpha}_{i,j}^H \mathbf{x}_j. \quad (2)$$

If the ith coordinate mapping vectors are found for all N channels, we can then obtain the *composite coordinate mapping* vector $\mathbf{a}_i = [\ \boldsymbol{\alpha}_{i,1}^H \ \ \boldsymbol{\alpha}_{i,2}^H \ \cdots \ \boldsymbol{\alpha}_{i,N}^H\ ]^H$ which is then used to find the *composite coordinate* vector $\mathbf{v}_i = [\ v_{i,1}^* \ \ v_{i,2}^* \ \cdots \ v_{i,N}^*\ ]^H = [\ \mathbf{x}_1^H \boldsymbol{\alpha}_{i,1} \ \ \mathbf{x}_2 \boldsymbol{\alpha}_{i,2} \ \cdots \ \mathbf{x}_N^H \boldsymbol{\alpha}_{i,N}\ ]^H$ which consists of the ith multi-channel coordinate of every channel. Note that * denotes the complex conjugate operation. The associated covariance matrix of $\mathbf{v}_i$ is given by

$$R_{\mathbf{v}_i\mathbf{v}_i} = E\left[\mathbf{v}_i \mathbf{v}_i^H\right] = \begin{bmatrix} \boldsymbol{\alpha}_{i,1}^H R_{11} \boldsymbol{\alpha}_{i,1} & \cdots & \boldsymbol{\alpha}_{i,1}^H R_{1N} \boldsymbol{\alpha}_{i,N} \\ \vdots & \ddots & \vdots \\ \boldsymbol{\alpha}_{i,N}^H R_{N1} \boldsymbol{\alpha}_{i,1} & \cdots & \boldsymbol{\alpha}_{i,N}^H R_{NN} \boldsymbol{\alpha}_{i,N} \end{bmatrix}.$$

Recall that in the two-channel CCA [5], [6], the correlations between the mapped coordinates are maximized subject to the constraint that the transformed coordinates have unit variance. In the multi-channel case, however, the analysis is not as well-defined as all correlations between all possible pairs of channels must be maximized simultaneously. To accomplish this, one approach that has been offered [7] is to maximize the sum of all correlations (the SUMCOR objective function) subject to the unit trace constraint of matrix $R_{\mathbf{v}_i\mathbf{v}_i}$. Thus, the optimization problem for finding the first composite coordinate mapping vector $\mathbf{a}_1$ using the objective function and constraint just described becomes

$$\mathbf{a}_1 = \arg\max_{\mathbf{a}_1} \sum_{j=1}^{N}\sum_{k=1}^{N} \boldsymbol{\alpha}_{1,j}^H R_{j,k} \boldsymbol{\alpha}_{1,k} = \arg\max_{\mathbf{a}_1} \sum_{j=1}^{N}\sum_{k=1}^{N} [R_{\mathbf{v}_1\mathbf{v}_1}]_{j,k} \quad (3)$$

subject to the constraint

$$\mathrm{tr}\left(R_{\mathbf{v}_1\mathbf{v}_1}\right) = \sum_{j=1}^{N} \boldsymbol{\alpha}_{1,j}^H R_{jj} \boldsymbol{\alpha}_{1,j} = 1,$$

It is shown [7] that the constrained optimization problem for the first coordinate mapping vectors, $\boldsymbol{\alpha}_{1,j}$ using a Lagrange multiplier method leads to

$$\sum_{k=1}^{N} R_{jk} \boldsymbol{\alpha}_{1,k} = \lambda_1 R_{jj} \boldsymbol{\alpha}_{1,j}, \quad \forall \ \ j,k \in [1,N]$$

or in matrix notation as

$$R_{\mathbf{zz}} \mathbf{a}_1 = \lambda_1 D \mathbf{a}_1, \quad (4)$$

where D is a block diagonal matrix with diagonal blocks $R_{jj} \ \ \forall \ \ j \in [1,N]$, i.e.

$$D = \mathrm{diag}\left[R_{11}, R_{22}, \ldots, R_{NN}\right]. \quad (5)$$

The result in (4) represents a generalized eigenvalue problem for which standard methods of solution are well-known. We will then consider the simultaneous solution to all mapping vectors $\mathbf{a}_i$'s, $i \in [1,d]$ and write (4) as $R_{\mathbf{zz}} A = DA\Lambda$ where A consists of all d coordinate mapping vectors, and Λ consists of all d eigenvalues. This solution can then be rewritten in terms of a standard eigenvalue problem $EP = P\Lambda$ where $E = D^{-\frac{1}{2}} R_{\mathbf{zz}} D^{-\frac{H}{2}}$ and P is a unitary matrix $\left(PP^H = P^H P = I\right)$. Clearly, we can find the mapping matrix A via $A = D^{-\frac{H}{2}} P$. Inspection of matrix E shows that it is simply the composite covariance matrix of the whitened version of $\mathbf{z} = [\ \mathbf{x}_1^H \ \cdots \ \mathbf{x}_N^H\ ]^H$. That is, if we define this whitened version of the composite data channel vector by $\mathbf{w} = [\ \mathbf{w}_1^H \ \cdots \ \mathbf{w}_N^H\ ]^H = D^{-\frac{1}{2}}\mathbf{z}$, then the whitened composite vector $\mathbf{w}$ has correlation matrix $E\left[\mathbf{w}\mathbf{w}^H\right] = D^{-\frac{1}{2}} R_{\mathbf{zz}} D^{-\frac{H}{2}} = E$. Matrix P is then used to map the whitened channels to their multi-channel coordinates. In order to find mapping vectors corresponding to the principal coordinates [7], we only consider the $r = d_1 = \min_j \{d_j\}$ coordinates such that $\lambda_1 > \lambda_2 > \ldots > \lambda_r$. Thus, $\Lambda = \mathrm{diag}\left[\lambda_1, \lambda_2, \ldots, \lambda_r\right]$ will become a $r \times r$ diagonal matrix composed of the dominant eigenvalues and P will become a

$d \times r$ matrix composed of the eigenvectors corresponding to r dominant eigenvalues. To find the mapped coordinate vector, $\mathbf{v}$, that contains all mapped coordinates for all N channels, we will first define Ψ_j (dimension $d_j \times r$) to contain those dominant r eigenvectors $\mathbf{p}_{i,j}$, $\forall\ i \in [1,r]$ of the mapping matrix P that correspond to the j^{th} channel

$$\Psi_j = \left[\ \mathbf{p}_{1,j} \quad \mathbf{p}_{2,j} \quad \cdots \quad \mathbf{p}_{r,j}\ \right],\ \forall\ j \in [1,N]. \tag{6}$$

Clearly, the connection between P and Ψ_j is evident

$$P = \begin{bmatrix} \Psi_1 \\ \Psi_2 \\ \vdots \\ \Psi_N \end{bmatrix}_{d \times r}. \tag{7}$$

Note that in the case of two channels, Ψ_1 and Ψ_2 are directly related to the mapping matrices of CCA [10]. All of the mapped coordinates of the jth channel can then be found by

$$\boldsymbol{\mu}_j = \Psi_j^H R_{jj}^{-\frac{1}{2}} \mathbf{x}_j,\quad \forall\quad j \in [1,N], \tag{8}$$

where $\boldsymbol{\mu}_j = \left[\ v_{1,j}^* \quad v_{2,j}^* \quad \cdots \quad v_{r,j}^*\ \right]^H$. Clearly, we have the following two properties

$$\begin{aligned} \sum_{j=1}^{N} E\left[\boldsymbol{\mu}_j \boldsymbol{\mu}_j^H\right] &= \sum_{j=1}^{N} \Psi_j^H \Psi_j = I \\ \sum_{j=1}^{N}\sum_{k=1}^{N} E\left[\boldsymbol{\mu}_j \boldsymbol{\mu}_k^H\right] &= \sum_{j=1}^{N}\sum_{k=1}^{N} \Psi_j^H R_{jj}^{-\frac{1}{2}} R_{jk} R_{kk}^{-\frac{H}{2}} \Psi_k = \Lambda \end{aligned}$$

If we define block diagonal matrix $\boldsymbol{\Psi}$ that contains the Ψ_j matrices along its diagonal blocks, i.e. $\boldsymbol{\Psi} = \text{diag}\left[\Psi_1, \Psi_2, \ldots, \Psi_N\right]$, then we can resolve all N channels into their multi-channel coordinates using

$$\mathbf{v} = \boldsymbol{\Psi}^H \mathbf{w} = \boldsymbol{\Psi}^H D^{-\frac{1}{2}} \mathbf{z}. \tag{9}$$

III. MCA Detection

A classical detection problem is that of choosing between two hypotheses that are relevant to the given problem. For this coherence-based detector, the null hypothesis (H_0) is the hypothesis that all N channels consist of background noise and the alternative hypothesis (H_1) that all N channels consist of signal plus noise. Figure 1 shows the graphical setup of the problem under consideration. Several simplifying but sensible assumptions used in this analysis are

1) Noise between different channels is mutually uncorrelated, i.e. $E\left[\mathbf{n}_j \mathbf{n}_k^H\right] = 0\ \forall\ j,k \in [1,N],\ j \neq k$.
2) Signal is uncorrelated with the background noise, i.e. $E\left[\mathbf{s}_j \mathbf{n}_k^H\right] = E\left[\mathbf{n}_j \mathbf{s}_k^H\right] = 0\ \forall\ j,k \in [1,N]$.
3) Noise contained on any one channel has covariance matrix, i.e. $E\left[\mathbf{n}_j \mathbf{n}_j^H\right] = R_{\mathbf{n}_j}\ \forall\ j \in [1,N]$.
4) Signal contained on any pair of channels has covariance matrix, i.e. $E\left[\mathbf{s}_j \mathbf{s}_k^H\right] = R_{\mathbf{s}_{jk}}\ \forall\ j,k \in [1,N]$.

Under H_0, the matrices $R_{\mathbf{zz}}$ and D become

$$R_{\mathbf{zz}_0} = D_0 = \text{diag}\left[R_{\mathbf{n}_1}, R_{\mathbf{n}_2}, \ldots, R_{\mathbf{n}_N}\right].$$

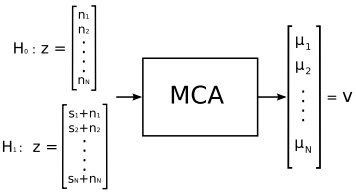

Fig. 1. Multi-Channel Hypothesis Test and MCA

Note that the subscript notation refers to the hypothesis being considered. Thus, the solution to the eigenvalue problem under H_0 leads to $\Lambda_0 = I$, while for A_0 no unique solution exists. Now, since any non-zero vector will satisfy the generalized eigenvalue problem, for simplicity we choose the eigenvectors of the null hypothesis to be the same as those of the alternative hypothesis, i.e. $A_0 = A_1 = A$.

Under H_1 and using the stated assumptions, the corresponding $R_{\mathbf{zz}}$ and D matrices are

$$\begin{aligned} R_{\mathbf{zz}_1} &= \begin{bmatrix} R_{\mathbf{s}_{11}} + R_{\mathbf{n}_1} & R_{\mathbf{s}_{12}} & \cdots & R_{\mathbf{s}_{1N}} \\ R_{\mathbf{s}_{21}} & R_{\mathbf{s}_{22}} + R_{\mathbf{n}_2} & \cdots & R_{\mathbf{s}_{2N}} \\ \vdots & \vdots & \ddots & \vdots \\ R_{\mathbf{s}_{N1}} & R_{\mathbf{s}_{N2}} & \cdots & R_{\mathbf{s}_{NN}} + R_{\mathbf{n}_N} \end{bmatrix} \\ D_1 &= \text{diag}\left[R_{\mathbf{s}_{11}} + R_{\mathbf{n}_1}, R_{\mathbf{s}_{22}} + R_{\mathbf{n}_2}, \ldots, R_{\mathbf{s}_{NN}} + R_{\mathbf{n}_N}\right] \end{aligned}$$

leading to the following arbitrary eigenvalue problem.

$$R_{\mathbf{zz}_1} A_1 = D_1 A_1 \Lambda_1 \tag{10}$$

The log-likelihood ratio that minimizes the risk involved in deciding between the two hypotheses is defined [5], [6] to be

$$l(\mathbf{z}) = \ln\left[\frac{p(\mathbf{z}|H_1)}{p(\mathbf{z}|H_0)}\right] \tag{11}$$

Assuming that under both hypotheses the composite data channel $\mathbf{z}$ is multivariate Gaussian with zero mean and covariance matrix $R_{\mathbf{zz}}$, the log-likelihood ratio of the composite data vector becomes

$$l(\mathbf{z}) = \mathbf{z}^H \left(R_{\mathbf{zz}_0}^{-1} - R_{\mathbf{zz}_1}^{-1}\right) \mathbf{z}. \tag{12}$$

Next, we can formulate $R_{\mathbf{zz}}^{-1}$ in terms of the sum of the correlations of each coordinate and their corresponding eigenvectors. To do this, we recall the fact that $P^H E P = \Lambda$. Taking the inverse of this relationship, it is simple to show that $R_{\mathbf{zz}}^{-1} = A \Lambda^{-1} A^H$. Thus, the log-likelihood function of (12) becomes

$$l(\mathbf{z}) = \mathbf{z}^H \left(A_0 \Lambda_0^{-1} A_0^H - A_1 \Lambda_1^{-1} A_1^H\right) \mathbf{z}.$$

Since the eigenvalues under the null hypothesis are all one, i.e. $\Lambda_0 = I$, and owing to the lack of a unique solution for the mapping matrices of the null hypothesis, we can write the log-likelihood ratio as

$$l(\mathbf{z}) = \mathbf{z}^H \left[A_1 \left(I - \Lambda_1^{-1}\right) A_1^H\right] \mathbf{z}, \tag{13}$$

where A_1 and Λ_1 are the mapping matrix and diagonal matrix of multi-channel correlations, respectively, for the set of data with which we are performing the hypothesis test.

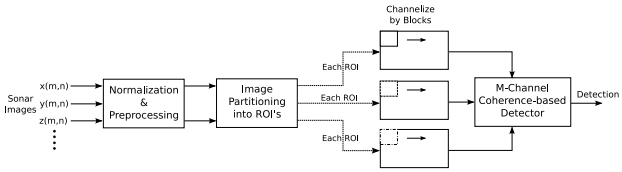

Fig. 2. Multiple Channel Detection System

Next, we will formulate the J-divergence [6] which is a measure of the separability of the two hypotheses. The J-divergence is defined to be

$$J = E_{H_1}\left[l(\mathbf{z})\right] - E_{H_0}\left[l(\mathbf{z})\right], \tag{14}$$

where $E_{H_1}[\,\cdot\,]$ and $E_{H_0}[\,\cdot\,]$ represent the expectation operation evaluated under the H_1 and H_0 hypotheses, respectively. The expected value of the log-likelihood function becomes

$$E\left[l(\mathbf{z})\right] = E\left[tr\left(\mathbf{z}^H Q \mathbf{z}\right)\right]. \tag{15}$$

Where $Q = \left(R_{\mathbf{zz}_0}^{-1} - R_{\mathbf{zz}_1}^{-1}\right)$. Using the cyclic property of the trace, we can write

$$\begin{aligned} E\left[l(\mathbf{z})\right] &= E\left[tr\left(Q\mathbf{z}\mathbf{z}^H\right)\right] \\ &= tr\left(QR_{\mathbf{zz}}\right). \end{aligned} \tag{16}$$

Thus, we can write the J-divergence as

$$\begin{aligned} J &= E_{H_1}\left[l(\mathbf{z})\right] - E_{H_0}\left[l(\mathbf{z})\right] \\ &= tr\left(QR_{\mathbf{zz}_1}\right) - tr\left(QR_{\mathbf{zz}_0}\right) \\ &= tr\left[-2I + R_{\mathbf{zz}_0}^{-1}R_{\mathbf{zz}_1} + R_{\mathbf{zz}_1}^{-1}R_{\mathbf{zz}_0}\right]. \end{aligned}$$

Rearranging and using the cyclic property of the trace, we can write the J-divergence as

$$= tr\left[-2I + \Lambda_1 + \Lambda_1^{-1}\right] = \sum_{i=1}^{r}\left(-2 + \lambda_i + \lambda_i^{-1}\right). \tag{17}$$

Therefore, the only pieces of information we need to know when performing detection in this framework are the matrices A_1 and Λ_1.

IV. Multi-Platform Test Results

The MCA-based coherence detector is applied to a four-platform sonar data set consisting of one HF high-resolution side-scan sonar image as well as three BB sonar images. For a review of HF and BB sonars, the reader is referred to [11] and [12]. As mentioned previously, multiple sensor detection is favorable over single platform detection as the detector has multiple independent looks at the same target thereby increasing the wealth of information available for the detection decisions. Because a HF sonar provides higher spatial resolution and better ability to capture target details and characteristics while a BB sonar offers much better clutter suppression ability with lower spatial resolution, detectors were run using HF images along with one or more of the BB sonars. Figure 2 exhibits the MCA-based detection system implemented for this data set when $N = 3$ channels are utilized. Three different cases were implemented, a two-channel detector with the HF sensor along with one BB sensor (HF-BB_1), a three-channel detector with the HF sensor, the same BB sensor, and another different BB sensor (HF-BB_1-BB_2), and finally a four-channel with the HF sensor, the same two BB sensors as before, and another different BB sensor (HF-BB_1-BB_2-BB_3). The goal of this study is to determine the impact different combinations and numbers of HF and BB sonar systems have on the detection performance and point of diminishing returns.

The image database used in this study contains 59 co-registered sonar images containing 53 targets with some of the images containing more than one target. The optimum ROI size was empirically chosen to be 72×112 pixels for the HF sonar images and 24×224 for all three of the BB sensors. The difference in size is due to the disparity in the spatial resolution of these sonar systems. Each sonar image is then partitioned into ROI's with a 50% overlap along both the range and cross-range directions. Each ROI is then channelized using a rectangular blocking scheme of which the dimensions are 6×4 and 2×8 for the HF and all three BB images, respectively. Using the MCA detector outlined in Section III, multi-channel correlations and mapping vectors are extracted for each ROI set.

To show the separability of the principal multi-channel correlations between ROI's that contain targets immersed in background and those that solely contain background, a test was conducted on the entire target set ROI's and a same size randomly selected set of ROI's containing only background clutter. Figures 3(a), (b), and (c) exhibit plots of the dominant 16 multi-channel correlations of ROI's containing targets and those solely containing background for the HF-BB_1, HF-BB_1-BB_2, and HF-BB_1-BB_2-BB_3 detectors, respectively. As can be seen, there is suitable separation among the principal correlation values pertaining to targets versus those pertaining to background alone. We can also observe that the more channels included for detection the higher the correlation values but this does not necessarily correspond to a subsequent increase in the separability among target and non target correlation values.

Next, for the detection process, the log-likelihood ratio expression in (12) was found for each block within an ROI set. A detection score was then created based on the percent of the log-likelihood measurements within an ROI set that fall below the detection threshold. A detection score of $\geq 50\%$ signifies the presence of a target within that set of ROI's. Figures 4(a), (b), and (c) show the histograms of the log-likelihood ratio values of one target ROI and one random background ROI for the HF-BB_1, HF-BB_1-BB_2, and HF-BB_1-BB_2-BB_3 cases, respectively. Using the entire set of target and background ROI's, an optimum threshold was experimentally determined to be 10.2 for all three detection cases. This threshold is shown by dotted vertical lines in Figures 4(a), (b), and (c).

All three detection systems are then implemented on the entire NSWC multi-platform sonar imagery data set using the predetermined threshold mentioned above. Table I lists the results of all three detectors. As one can see, the two-channel (HF-BB_1) detector performs marginally well with

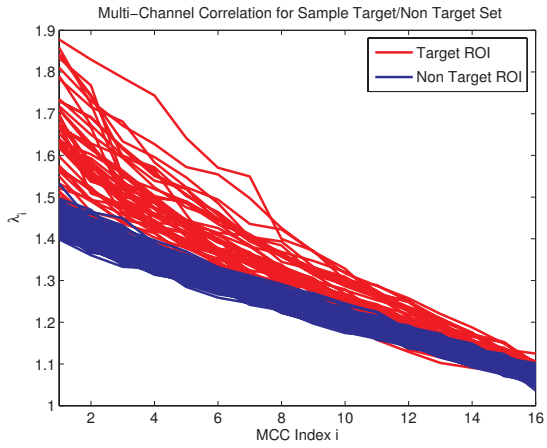

(a) HF-BB_1 Detector

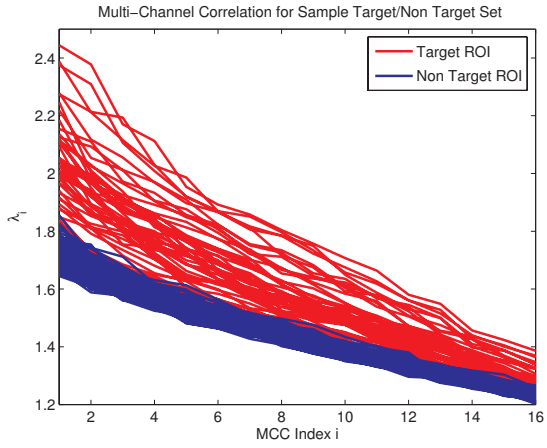

(b) HF-BB_1-BB_2 Detector

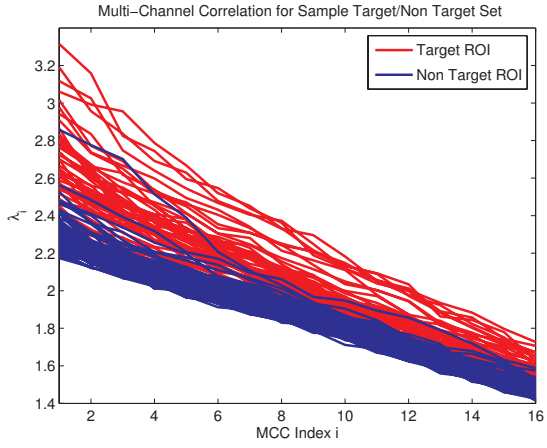

(c) HF-BB_1-BB_2-BB_3 Detector

Fig. 3. Plot of Multi-Channel Correlations for Target and Background for all Three Detectors.

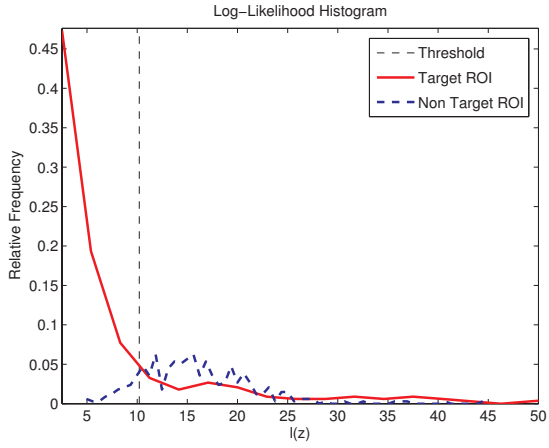

(a) HF-BB_1 Detector

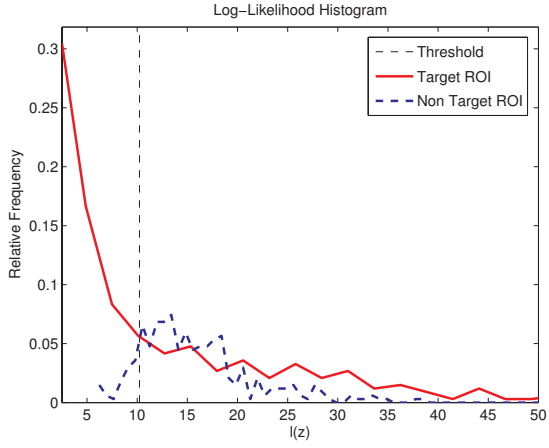

(b) HF-BB_1-BB_2 Detector

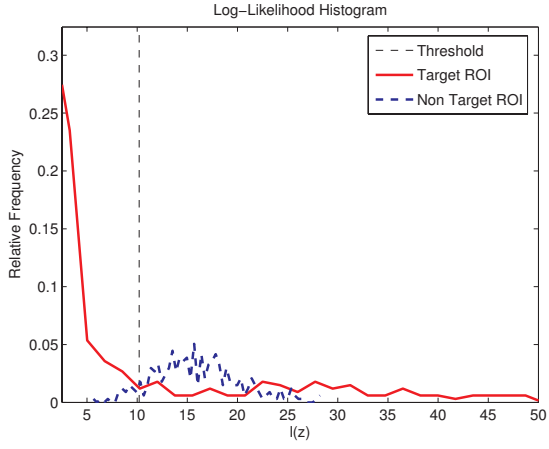

(c) HF-BB_1-BB_2-BB_3 Detector

Fig. 4. Histogram of Example Log-Likelihood Values for Target and Background for all Three Detectors.

TABLE I
MULTI-PLATFORM DETECTION RESULTS

Detector	Targets Detected (Out of 53 Targets)	Average False Detections per Image
HF-BB_1	51	7.48
HF-BB_1-BB_2	52	8.93
HF-BB_1-BB_2-BB_3	52	9.32

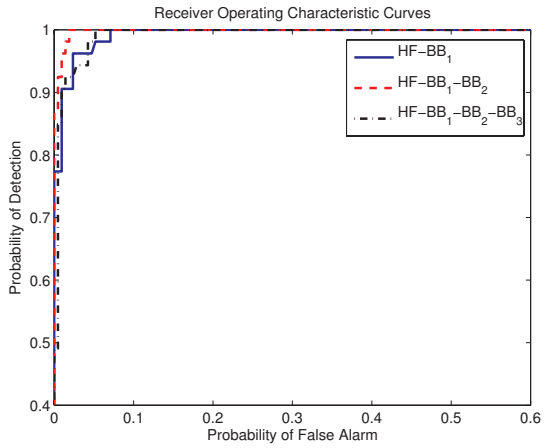

Fig. 5. ROC Curves for all Three Detectors

more than 90% of the targets being detected and less than 10 false alarms per image. The three (HF-BB_1-BB_2) and four-channel (HF-BB_1-BB_2-BB_3) detectors subsequently seem to perform better as they both detect more of the targets while still maintaining a low false alarm rate. The ROC curves for all three detectors are presented in Figure 5. Again, we can see that the three-channel detector provides an increase in performance over that of the two-channel detector as the two-channel detector exhibits $P_d = 96\%$ and $P_{fa} = 4\%$ at the knee point of the ROC curve whereas that of the three-channel detector gives $P_d = 98\%$ and $P_{fa} = 2\%$. However, the performance of the four-channel detector actually decreases with $P_d = 96\%$ and $P_{fa} = 4\%$ at the knee point of the ROC curve. This decrease in detection performance as you go from the three to the four-channel detector could possibly suggest the point of diminishing returns as the BB-3 sonar did not bring any new pertinent information of the targets and actually worsens the performance by increasing the number of false alarms. This could be due to the fact that increasing the number of broadband sonar platforms that essentially contain similar target information smears the overall coherence as the correlations become less representative and more deficient. However, because of the small number of targets present within the data set, it is hard to say with any confidence whether this is the actual underlying response of the detector or not. Both the HF-BB_1-BB_2 and HF-BB_1-BB_2-BB_3 detectors missed the same target. However, the HF-BB_1 detector missed two other targets, neither of which are the same target as that missed by the three and four channel detectors. The targets missed by these detection systems were faint in signature and hard to visually discern in all images hence leading to low coherence and subsequent misdetection. Overall, all the detection systems tested performed extremely well given the small number of targets and non targets used to form the detection threshold.

V. CONCLUSION

A new multi-channel, multi-sensory binary hypothesis detection system has been introduced using the MCA framework. An N-channel Gauss-Gauss detector is then formulated in the MCA coordinates. Detection is performed by extracting the multi-channel mapping vectors and the correlation sums from the data samples collected by the sensory platforms. These mapping vectors and coherent features are then used in the log-likelihood ratio to detect targets in the sonar images. This MCA-based detector is then applied to a disparate sonar data set consisting of one HF sonar and three BB sonars. Three different MCA-based detectors were implemented and applied to this data set and their performances compared to determine optimal combinations and number of sonar channels. All three detectors performed exceptionally well with probability of detections greater than 95% and probability of false alarms at less than 5%. Through this work we have shown that MCA provides a robust and elegant framework when attempting to perform coherence-based detection among multiple disparate sensory channels.

ACKNOWLEDGMENT

This work was supported by the Office of Naval Research, Code 321OE under contract #N00014-08-1-0142

REFERENCES

[1] G. J. Dobeck, J. Hyland, and L. Smedley, "Automated detection/classification of sea mines in sonar imagery," *Proc. SPIE*, vol. 3079, pp. 90–110, April 1997.
[2] T. Aridgides, P. Libera, M. Fernandez, and G. J. Dobeck, "Adaptive filter/feature orthogonalization processing string for optimal LLRT mine classification in side-scan sonar imagery," *Proc. SPIE*, vol. 2765, pp. 110–121, April 1996.
[3] T. Aridgides and M. Fernandez, "Enhanced atr algorithm for high resolution multi-band sonar imagery," *Proc. SPIE*, vol. 6953, pp. 0H1–0H10, March 2008.
[4] J. D. Tucker, N. Klausner, and M. R. Azimi-Sadjadi, "Target detection in m-disparate sonar platforms using multichannel hypothesis testing," *Proc. of MTS/IEEE Oceans 2008 Conference*, to be published.
[5] A. Pezeshki, L. Scharf, J. Thomas, and B. Van Veen, "Canonical coordinates are the right coordinates for low-rank gauss-gauss detection and estimation," *IEEE Transactions on Signal Processing*, vol. 54, pp. 4817–4820, December 2006.
[6] L. Scharf and B. Van Veen, "Low rank detectors for gaussian random vectors," *IEEE Transactions on Acoustics, Speech, and Signal Processing*, vol. 35, pp. 1579–1582, November 1987.
[7] B. Thompson and M. Azimi-Sadjadi, "Iterative multi-channel coherence analysis with applications," *Neural Networks*, vol. 21, pp. 493–501, 2008.
[8] H. Hotelling, "Relations between two sets of variates," *Biometrika*, vol. 28, pp. 321–377, 1936.
[9] A. Rencher, *Methods of Multivariate Analysis*, 2nd ed. Wiley-Interscience, 2002.
[10] L. Scharf and C. Mullis, "Canonical coordinates and the geometry of inference, rate, and capacity," *IEEE Transactions on Signal Processing*, vol. 48, pp. 824–831, March 2000.
[11] W. Key, "Side scan sonar technology," *Proc. Oceans'00*, vol. 2, pp. 1029–1033, Sept 2000.
[12] S. Butler, "Triply resonant broadband transducers," *Oceans '02 MTS/IEEE*, vol. 4, pp. 2334–2341 vol.4, 29-31 Oct. 2002.